Open Archive TOULOUSE Archive Ouverte (OATAO)
OATAO is an open access repository that collects the work of Toulouse researchers and makes it freely available over the web where possible.

This is an author-deposited version published in : http://oatao.univ-toulouse.fr/
Eprints ID : 15689

To link to this article : DOI:10.1016/j.ces.2015.01.070
URL : http://dx.doi.org/10.1016/j.ces.2015.01.070

To cite this version : Dorai, Ferdaous and Moura Teixeira, Carlos and Rolland, Matthieu and Climent, Eric and Marcoux, Manuel and Wachs, Anthony *Fully resolved simulations of the flow through a packed bed of cylinders: Effect of size distribution.* (2015) Chemical Engineering Science, vol. 129. pp.180-192. ISSN 0009-2509

Any correspondence concerning this service should be sent to the repository administrator: staff-oatao@listes-diff.inp-toulouse.fr

Fully resolved simulations of the flow through a packed bed of cylinders: Effect of size distribution

Ferdaous Dorai [a], Carlos Moura Teixeira [a], Matthieu Rolland [a], Eric Climent [b], Manuel Marcoux [b], Anthony Wachs [c,]

[a] IFP Energies nouvelles, Process Intensification Department, Rond-point de l'Echangeur de Solaize, BP 3, 69360 Solaize, France
[b] Institut de Mécanique des Fluides de Toulouse, 2 Allée du Professeur Camille Soula, 31400 Toulouse, France
[c] IFP Energies nouvelles, Fluid Mechanics Department, Rond-point de l'Echangeur de Solaize, BP 3, 69360 Solaize, France

HIGHLIGHTS

- 3D fully resolved simulations of the flow through a packed bed of cylinders.
- Satisfactory accuracy at high solid fraction without any hydrodynamic radius calibration.
- Effect of bed microstructure (particle shape, polydispersity) on pressure drop.
- Discussion and comparison with existing pressure drop correlations.

GRAPHICAL ABSTRACT

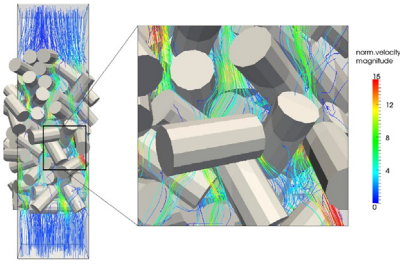

ABSTRACT

Fully resolved simulations of the flow through a fixed bed of pellets are performed to better understand the effect of the local microstructure on the energy loss, i.e., pressure drop through the bed. Both mono-disperse and poly-disperse systems as well as spherical and cylindrical pellets (solid particles) are investigated. Using a DEM-DLM/FD simulation method inspired by "Wachs, A. (2009). A DEM-DLM/FD method for direct numerical simulation of particulate flows: sedimentation of polygonal isometric particles in a Newtonian fluid with collisions. Comput. Fluids 38(8), 1608–1628" and implemented here in a Finite Volume context with second order reconstruction of the particle boundary as in "Rahmani, M., Wachs, A. (2014). Free falling and rising of spherical and angular particles. Phys. Fluids 26, 083301", we evidence that the computed solution converges nicely with mesh refinement and provide guidelines on the grid size to guarantee a satisfactory level of accuracy. Based on these trustworthy simulation results, we investigate the impact of the particle shape as well as the degree of poly-dispersity in the system on the pressure drop over the fixed bed in the viscous regime. Unprecedented simulation results on the flow through a bed of poly-disperse cylinders indicate that the correlation for poly-disperse spheres suggested in "Van der Hoef, M.A., Beetstra, R., Kuipers, J.A.M. (2005). Lattice-Boltzmann simulations of low-Reynolds-number flow past mono- and bidisperse arrays of spheres: results for the permeability and drag force. J. Fluid Mech. 528, 233–254" may still be valid for cylinders of moderate aspect ratio.

Keywords:
Packed bed
Catalyst reactor
Granular dynamics
Particulate flow
Parallel computing

1. Introduction

Most catalytic refining and petrochemical reactions are operated with fixed bed reactors. In these reactors, catalyst pellets are generally randomly stacked in a large cylindrical vessel and the reactants,

usually gas and liquid, are flowing through the bed to react inside the catalyst pellets. Catalyst pellets are made of a porous support onto which are deposited active materials (noble metals, sulphides, etc.). They are typically from 0.2 to 5 mm in size with spherical, cylindrical or more complex shapes (tri-lobic or quadri-lobic extrudates). Overall pellet activity depends on support (pore size distribution, physico-chemical properties like acidity) and also on active phase properties (dispersion, amount of metals, size of crystallites, depth of penetration in the support, etc.).

Traditional trends in the chemical industry have always been towards more economical processes, that is more active, longer lasting catalysts in combination with more efficient processes. More efficient processes can be designed based on a better comprehension of the physics ruling reactor performances in terms of chemical but also thermal and mechanical (pressure drop) responses. A finer representation of the catalytic process allows smaller over-designs and a better integration with other equipment (including resistance to pollutants, etc.). Thus, catalyst development has been more and more concerned with the acquisition of accurate knowledge that can be up-scaled to industrial design, thus requiring better reactors and better analytical techniques.

Designing a new catalyst requires the ability to manufacture numerous small batches of catalyst prototype and assess their performances on simulated or real feedstocks. Assessing the catalyst performance is performed in pilot units at pressure and temperature similar to those of the industry for thermodynamic reasons. Historically, pilot unit reactor technology has been chosen to match that of the industrial processes: the idea is that keeping the same technology should make the physics unchanged and thus result in a straightforward up-scaling. Development cost and delays can be reduced if the amount of prototype catalyst to be tested is reduced. Fixed bed pilot unit sizes have thus been decreasing steadily over the years: from units requiring a few litres of catalyst in the 80s to a current range of 0.1–50 ml reactor volume.

Size reduction, or down-scaling of pilot unit has been a major challenge in the recent years. Sie (1991) proposed a comprehensive review on the subject. Major down-scaling issues are change in mass transfer from fluid to catalyst pellets, change in overall reactor hydrodynamic (axial dispersion).

Universally, up-scaling is based on the conservation of the "residence time" in the reactor or its inverse, the LHSV (Liquid Hourly Space Velocity) defined as the flow-rate of feedstock divided by the catalyst volume (expressed in 1/h). LHSV can be rewritten as the ratio of the superficial velocity to the length of reactors. Industrial reactors are typically 5–30 m long. Such length is not compatible with a laboratory environment: velocities in the pilot units are 10 to 100 times slower than in industrial plants (Sie, 1991). This decrease in velocities has been shown to have a significant negative effect on external mass transfer rate, that is the ability of the reactor to supply the catalyst with reactants. A comprehensive review on mass transfer has been written by Dudukovic et al. (2002). Another consequence of velocity reduction is a drastic change in flow patterns and especially a decrease in the wetted area of catalyst pellets. Solutions proposed in the 90s have been to operate in upflow (bubble flow mode) or to fill up the porosity with fine inert powder that promotes full wetting (Sie, 1991).

Another drawback of size reduction is the potential loss of the plug-flow behaviour. In industrial fixed bed reactors, molecules exit the reactor in the same order as they enter: this is ideal plug-flow. In small size reactors, the residence time distribution is not ideal: some molecules stay longer than the average, some molecules stay shorter. A common explanation is related to the increased importance of wall effects: near the reactor walls, the overall bed porosity is significantly higher than in the centre of the reactor leading to bypass flows of reactants in a region of a typical width of 2–3 diameters (Giese et al., 1998). As the reactor diameter decreases, while keeping the catalyst pellets unchanged, the wall effect gains in relative intensity. Small deviation from ideality can be described using a dispersive plug-flow model, in which a dispersion term is used to represent all the non-ideality. A review on dispersion has been proposed by Delgado (2006). Dispersive behaviour means that contact time with catalyst pellets depends on each path in the reactor: conversion is not identical on all paths so that the apparent reactor performance is an average of the activity on each path. For very high conversion reactions, assessment of catalyst activity or even target performance may not be achieved. The higher the conversion, the more plug-flow the reactor should be (Gierman, 1988). As in small scale fixed beds, dispersion depends on the ratio of reactor length to particle diameter (Delgado, 2006; Sie, 1991), plug flow behaviour can be achieved by filling up the space between catalyst pellets by fine inert powder (Sie, 1991).

Interestingly, it has been observed that at very low tube to particle diameter ratio (below 7–10), dispersion is smaller than for larger (in the sense higher tube to particle diameter ratio) reactors (Knox and Parcher, 1969). This is known as the Knox Parcher effect. For small reactors, there is no porosity difference near the wall and the centre: the pellets packing structure becomes quite uniform. Theoretical statistical considerations (Dagan, 1989) indicate also that a minimum bed height of about 15 particle diameters is required for dispersive plug-flow model to be valid. Below this length, the theory indicates that random effects should predominate. Recently, we proved using direct numerical simulation (DNS) of reactive flow in a box containing 8 cylinders (Rolland, 2013) that orientation and position of catalyst pellets could change significantly the apparent reactor performance. Further size reduction requires to rethink traditional chemical engineering fixed bed design rules and to investigate local effects, namely the interaction at pellet scale of pellet position and orientation (random) with flow and reactant transport.

Computing the detailed kinematics of the flow through a porous media is not an easy task for the two following primary reasons:

(1) the domain geometry is quite intricate which leads to issues in generating the mesh of the computational fluid domain, and
(2) creating the geometry, i.e., the assembly of pellets (solid particles), itself, is not straightforward.

For the latter, one common option in the literature is to perform a dynamic granular simulation of the filling stage, i.e., as particles are poured into the container, all particle–particle and particle–wall collisions are calculated. This type of method is not only efficient in the sense that it supplies a realistic assembly of particles but also mimics the filling process and hence allows one to investigate the influence of the type of filling process on the final microstructure of the assembly of particles (porosity, tortuosity, local defects, etc.). Among the various computational methods available to simulate granular dynamics (Event-Driven method, Non-Smooth Contact Dynamics, Discrete Element, etc.), the Discrete Element Method (DEM) (Cundall and Strack, 1979) is likely to be the most commonly used, with hundreds of publications in the international literature every year. DEM is conceptually simple and easy to implement for spherical particles, and has been shown to yield physically sensible results. Its extension to non-spherical and angular particles is however more complicated in relation to the determination of the network of contacts. It is primarily a geometric problem. Fortunately, various collision detection techniques have been devised to account for non-smooth shapes (see, e.g., Kodamn et al., 2010 for a review of these techniques), and among them the one suggested by our group and based on the use of a Gilbert–Johnson–Keerthi (GJK) algorithm for

the geometric detection of the contact points (Wachs et al., 2012). Our numerical code, Grains3D, has been validated in assorted granular flow configurations and in particular enables one to fill a container with any kind of convex shapes (Wachs et al., 2012; Dorai et al., 2012a).

For the former, there are essentially two main options to proceed: (i) creating a boundary fitted unstructured mesh and solving the fluid problem in the fluid domain only, with no slip boundary conditions at the particle surface or (ii) employing a regular simple structured mesh and account for the presence of the fixed particles treated as obstacles by forcing the fluid velocity to locally be zero. Solution (i) constitutes the traditional way of examining this type of flow (Atmakidis and Kenig, 2012; Combest et al., 2012; Dixon et al., 2010), its advantage being the ability to refine the mesh wherever necessary (e.g., the boundary layer close to the particle surface) while it requires to generate a new mesh anytime the microstructure changes (which can be a tedious process and might necessitate a very sophisticated meshing tool). Solution (ii) belongs to the class of non-boundary fitted methods like Immersed Boundary (IBM) (Peskin, 1977; Uhlmann, 2005), lattice-Boltzmann (LBM) with bounce-back collision rule at particle boundary (Van der Hoef et al., 2005; Hill et al., 2001a, 2001b; Graf von der Schulenburg and Johns, 2011), Distributed Lagrange Multiplier/Fictitious Domain (DLM/FDM) (Glowinski et al., 1999; Yu and Shao, 2007; Wachs, 2009, 2011), or Force Coupling (FCM) (Climent and Maxey, 2003), to name the most popular ones only. Each of the four aforementioned methods (IBM, LBM, DLM/FDM, FCM) has been applied with reasonable success to a variety of flow configurations (including both fixed and moving solid particles). Here, we use PeliGRIFF (*Parallel Efficient LIbrary for GRains In Fluid Flow*), the DLM/FDM based parallel flow solver developed in our group (Wachs, 2009, 2011). We shall evidence later in the paper that the combination of Grains3D and PeliGRIFF is an appropriate computational strategy to compute the flow and the pressure drop in a packed bed of cylinders.

The rest of the paper is organized as follows. Section 2 gives a short presentation of our two numerical tools together with validations of our DLM/FDM on low porosity problems with spheres. Then, we analyse in Section 3 the flow through a loosely packed bed of cylinders. In particular, we assess the effect of size distribution on the pressure drop through the bed and discuss the validity of the extension of the correlation of Van der Hoef et al. (2005), Beetstra et al. (2007) and Sarkar et al. (2009) proposed for spheres to cylinders for the estimation of the pressure drop. Finally, we sum up in Section 4 our results and list the perspectives on the present study.

Remark. To avoid any misunderstanding, all dimensional quantities are denoted throughout the rest of the paper with a superscript "*".

2. Numerical model

For the sake of clarity, we shortly present below the numerical methods we employ to simulate the flow through the packed bed of cylinders. We use two different solvers: the former enables us to construct the pack of solid particles and the latter computes the flow through the packed bed. For a more detailed presentation of these two numerical tools, the reader is referred to the publications cited in the two following sub-sections.

2.1. Granular solver

Creating a packed bed of solid particles in not an easy task, especially for non-spherical particles. Besides, even for spheres, it is far from being entirely straightforward. There are essentially two options: (i) using a classical Monte Carlo procedure to distribute the spheres in the domain until the desired compacity is reached, or (ii) performing an actual dynamic granular simulation under controlled conditions of the pouring process of the particles in the domain and letting the system relax to rest. We chose the latter option for two primary reasons: (i) it is much more versatile in the sense that it can be extended to non-spherical shapes and (ii) it is physically more sensible since it models an actual granular flow.

Our granular solver is based on the Discrete Element Method (DEM) (Cundall and Strack, 1979) and a soft-sphere collision model. The soft-sphere collision model implies to allow the rigid particles to slightly overlap as they touch and to use a geometric measure (usually a distance) of the overlap to calculate the contact forces. The contact force model considered in all our simulations is very standard: its mechanical analog is a Hookean spring and a dashpot in the normal direction and a dashpot and a Coulomb frictional element that limits the force to its Coulomb upper bound in the tangential direction (Wachs et al., 2012). Other more sophisticated alternatives exist (see, e.g., Dviugys and Peters, 2001 for a comprehensive overview). Each collision between two nearby particles is numerically integrated over time, leading to time steps much smaller than the physical contact time. DEM is not limited to binary collisions and collisions between multiple particles are addressed without any particular trouble.

The motion of the granular material is determined by applying Newton's second law to each particle $i \in \langle 0, N-1 \rangle$, where N is the total number of particles. Since particles are rigid, their velocity vector $\boldsymbol{v}^*$ satisfies $\boldsymbol{v}^* = \boldsymbol{U}^* + \boldsymbol{\omega}^* \wedge \boldsymbol{R}^*$, where $\boldsymbol{U}^*$, $\boldsymbol{\omega}^*$ and $\boldsymbol{R}^*$ denote the translational velocity vector, the angular velocity vector and the position vector with respect to the center of mass, respectively. This decomposition classically leads to a force equation for $\boldsymbol{U}^*$ and a torque equation for $\boldsymbol{\omega}^*$. The complete set of equations to be considered is the following one:

$$M_i^* \frac{d\boldsymbol{U}_i^*}{dt^*} = \boldsymbol{F}_i^* \tag{1}$$

$$\boldsymbol{J}_i^* \frac{d\boldsymbol{\omega}_i^*}{dt^*} + \boldsymbol{\omega}_i^* \wedge \boldsymbol{J}_i^* \boldsymbol{\omega}_i^* = \boldsymbol{M}_i^* \tag{2}$$

$$\frac{d\boldsymbol{x}_i^*}{dt^*} = \boldsymbol{U}_i^* \tag{3}$$

$$\frac{d\boldsymbol{\theta}_i^*}{dt^*} = \boldsymbol{\omega}_i^* \tag{4}$$

where M_i^*, $\boldsymbol{J}_i^*$, $\boldsymbol{x}_i^*$ and $\boldsymbol{\theta}_i^*$ stand for the mass, inertia tensor, center of mass position and angular position of particle i, respectively. $\boldsymbol{F}_i^*$ and $\boldsymbol{M}_i^*$ are the sum of all forces and torques applied on particle i, respectively. In our study, only gravity and contact forces act on a particle; thus $\boldsymbol{F}_i^*$ and $\boldsymbol{M}_i^*$ can be further decomposed as

$$\boldsymbol{F}_i^* = M_i^* \boldsymbol{g}^* + \sum_{j=0, j \neq i}^{N-1} \boldsymbol{F}_{ij}^* \tag{5}$$

$$\boldsymbol{M}_i^* = \sum_{j=0, j \neq i}^{N-1} \boldsymbol{R}_j^* \wedge \boldsymbol{F}_{ij}^* \tag{6}$$

where $\boldsymbol{g}^*$ is the gravity acceleration vector, $\boldsymbol{R}_j^*$ a vector pointing from the center of mass of particle i to the contact point with particle j and $\boldsymbol{F}_{ij}^*$ the contact force vector.

In our code, Grains3D, we use a sophisticated collision detection strategy based on a Gilbert–Johnson–Keerthi (GJK) distance algorithm (Gilbert et al., 1988; Van den Bergen, 1999) that enables us to examine any kind of combination of convex particle shapes and sizes (as illustrated in Fig. 1 where various convex shapes are packed in a cylindrical container). For a detailed description of

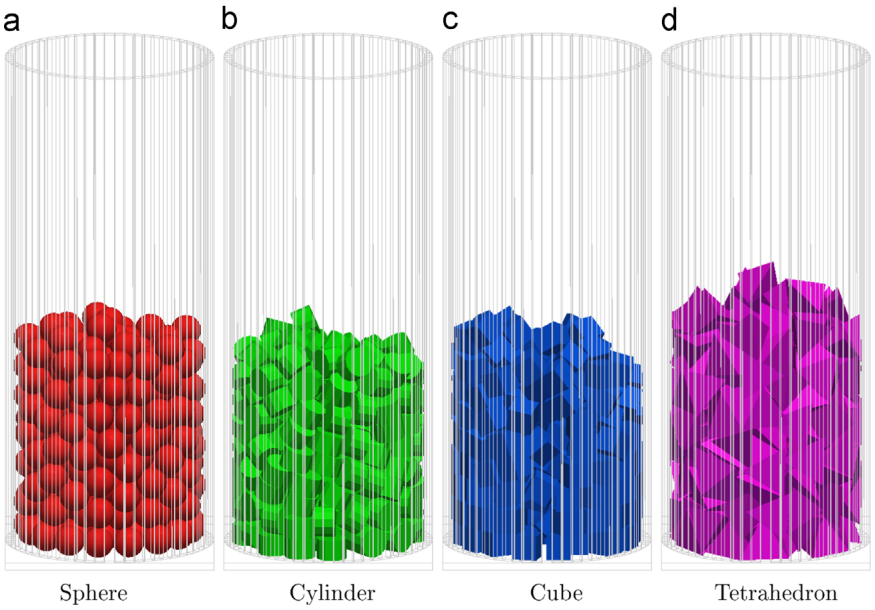

Fig. 1. Packing of different shapes in a cylindrical container with Grains3D. (a) Sphere, (b) cylinder, (c) cube and (d) tetrahedron.

Grains3D, the reader is referred to Wachs et al. (2012). Here, we apply Grains3D to a polydisperse set of 3D cylindrical particles.

2.2. Flow solver around the fixed particles

The DLM/FD method used in our code PeliGRIFF implies to use a cartesian structured mesh of constant grid size, to solve the fluid conservation equations everywhere in the domain and to force the rigid body motion (motionless in the particular case of the application treated in this paper) in the regions (filled of fictitious fluid) occupied by the particles (Glowinski et al., 1999; Yu and Shao, 2007; Wachs, 2009, 2011). Assorted variants at the discrete level have been suggested in the literature. Here, we combine the DLM/FDM with a Finite Volume/Staggered Grid discretization scheme for the fluid equations, an implicit solution of the resulting DLM/FD saddle-point problem by a Uzawa algorithm, a collocation-point method to discretize the particles on the fluid mesh and a second-order interpolation on the fluid velocity at the particle boundary (Rahmani and Wachs, 2014). Further detail can be found in Wachs et al. (2015).

Even in steady situations, the flow solution is obtained as the steady state of a time evolving problem. The solving algorithm is of the operator-splitting type and comprises two stages as follows, where governing equations are written in a dimensionless form:

(1) A classical L2-projection scheme for the solution of the Navier-Stokes problem: find $\boldsymbol{u}^{n+1/2}$ and p^{n+1} such that

$$\frac{\tilde{\boldsymbol{u}}-\boldsymbol{u}^n}{\Delta t}-\frac{1}{2\,\mathcal{R}e}\nabla^2\boldsymbol{u}^{n+1/2}=-\nabla p^{n+1}+\frac{1}{2\,\mathcal{R}e}\nabla^2\boldsymbol{u}^n,$$
$$-\frac{1}{2}(3\boldsymbol{u}^n\cdot\nabla\boldsymbol{u}^n-\boldsymbol{u}^{n-1}\cdot\nabla\boldsymbol{u}^{n-1})-\alpha\boldsymbol{\lambda}^n, \tag{7}$$

$$\nabla^2\psi=\frac{1}{\Delta t}\nabla\cdot\tilde{\boldsymbol{u}},\quad \frac{\partial\psi}{\partial n}=0 \text{ on } \partial\Omega, \tag{8}$$

$$\boldsymbol{u}^{n+1/2}=\tilde{\boldsymbol{u}}-\Delta t\nabla\psi,$$
$$p^{n+1}=p^n+\psi-\frac{\Delta t}{2\,\mathcal{R}e}\nabla^2\psi. \tag{9}$$

(2) A fictitious domain problem: find $\boldsymbol{u}^{n+1}$ and $\boldsymbol{\lambda}^{n+1}$ such that

$$\frac{\boldsymbol{u}^{n+1}-\boldsymbol{u}^{n+1/2}}{\Delta t}+\boldsymbol{\lambda}^{n+1}=\alpha\boldsymbol{\lambda}^n, \tag{10}$$

$$\boldsymbol{u}^{n+1}=\boldsymbol{0}\quad \text{in } P(t). \tag{11}$$

where $\boldsymbol{u}$, $\tilde{\boldsymbol{u}}$, p, λ, ψ and Δt denote the dimensionless fluid velocity vector, non-divergence-free predicted fluid velocity vector, fluid pressure, DLM/FD Lagrange multiplier to relax the constraint (11), pseudo-pressure field and time step, respectively. Ω and $\partial\Omega$ represent the flow domain and its boundary, respectively, and $P(t)$ the region occupied by the particles. $\alpha\in[0:1]$ enables one to add explicit direct forcing at the velocity prediction step (7). Setting $\alpha=1$ significantly improves the coupling between sub-problems (1) and (2) and allows for larger time steps Δt. In practice, all computations are performed with $\alpha=1$ (see Wachs et al., 2015 for more detail). Finally, $\mathcal{R}e$ stands for the Reynolds number and reads

$$\mathcal{R}e=\frac{\rho_f^*U_c^*L_c^*}{\eta^*} \tag{12}$$

where ρ_f^*, U_c^*, L_c^* and η^* are the fluid density, characteristic velocity, characteristic length and fluid viscosity, respectively. In the case of the flow through a fixed bed of particles, obvious choices for U_c^* and L_c^* are the fluid inlet velocity and the equivalent particle diameter, but other choices are also conceivable.

Our objective is to examine the flow through a fixed bed of cylinders at a low but finite Reynolds number (laminar and steady regime). However, simulating this type of flow at a low porosity (less than 0.5) with a reasonably good accuracy still represents a challenging problem for non-boundary fitted methods like IBM, LBM, DLM/FDM or FCM. Hence, we first validate our method by comparing our computed results with analytical exact solutions and other numerical data from the literature on problems involving spheres. In particular, we evidence that our method, unlike other works using IBM or LBM, does not require any hydrodynamic radius calibration and provides satisfactory solutions with the actual (geometric) particle

radius. This allows us to then extend our study to cylinders and simply use their actual geometric features (diameter and height).

2.3. Validation of the method on the flow through a periodic array of spheres: Stokes and inertial regimes, structured and random arrays

The DLM/FDM has already been validated in numerous flow configurations in the past literature (Glowinski et al., 1999; Yu and Shao, 2007; Wachs, 2009, 2011) but very often in dilute regimes. As the solid volume fraction increases, the accuracy of the computed solution deteriorates and predictions show a large discrepancy unless an adequate remedy is devised. In most IBM and LBM works, the hydrodynamic radius is adjusted such that the numerical method properly predicts the hydrodynamic force experienced by a spherical particle in a dilute regime. The calibrated or effective hydrodynamic radius (slightly larger than the actual geometric radius in LBM, Van der Hoef et al., 2005; Hill et al., 2001a,b; Ladd and Verberg, 2001; while slightly lower in IBM, Höfler and Schwarzer, 2000; Breugem, 2012) is then used as well in more concentrated and/or inertial regimes. Though this calibration procedure has permitted to supply valuable information on the flow through structured and random array of spheres, it is still somehow questionable, in the sense that it is not clear what is the motivation to perform this calibration, except to correct an intrinsic drawback of the numerical method. Recently, Deen et al. (2012) have suggested another fully resolved numerical method that provides satisfactory results up to high solid volume fraction (low porosity) that does not rely on any calibration procedure of the hydrodynamic radius. In our code PeliGRIFF, we follow the same guideline and hence highlight below that using a second-order outwards-oriented interpolation (as in a Q2 quadratic finite element) instead of a classical multi-linear one of the fluid velocity at the particle boundary allows us to supply accurate results, though we consider the actual radius. A set of DLM/FD points and the two types of interpolation (multi-linear and quadratic) are illustrated in Fig. 2 in 2D for a circular cylinder.

The first test case is the flow through an infinite structured simple cubic array of spheres at $\mathcal{R}e = 0$. This problem is a very appropriate candidate to validate our code since it possesses an exact analytical solution derived in Zick and Homsy (1982) up to the maximum structured packing $\phi_{max} = \pi/6 \simeq 0.524$, where $\phi = 1 - \epsilon$ is the solid volume fraction and ϵ the porosity. In our simulations, the system is modelled as follows: a single sphere is set at the center of a cubic computational domain with periodic boundary conditions in all 3 directions. A pressure drop is imposed in one of the 3 directions, e.g. x, and the resulting flow rate Q^* is measured. Following Zick and Homsy (1982), the relation between the mean velocity V^* and the imposed pressure drop ΔP^* involves a drag coefficient K and is defined as follows:

$$\frac{\Delta P^*}{L^*} = \frac{9}{2}\frac{\eta^*}{a^{*2}}\phi K V^* \tag{13}$$

where L^* and a^* denote the cube edge length and sphere radius, respectively, and $V^* = Q^*/L^{*2}$. Zick and Homsy (1982) supply the analytical evolution of K as a function of ϕ. We plot in Fig. 3(a) the solution computed by PeliGRIFF for a $40 \times 40 \times 40$ mesh and a dimensionless time step $\Delta t = 0.01$. This plot evidences a very satisfactory agreement with the analytical solution in Zick and Homsy (1982) up to $\phi_{\max}$, the maximum error being less than 3%. We further examine the accuracy of our computed solution in Fig. 3(b) by plotting its convergence as a function of N_p, the number of DLM/FD points on the particle diameter (that varies as $1/h$, h being the grid size). This plot leads to the three following comments:

(1) for all ϕ, we get a clean and nice spatial convergence,
(2) generally the solution converges as N_p^{α} with $\alpha \in [1 : 1.5]$, which is deemed to be satisfactory for a second-order accurate scheme for a fluid flow without particles and a non-boundary fitted treatment of the particles. And again, we point out that no effective hydrodynamic radius or calibration procedure is employed. The radius of the sphere in our simulations is simply its geometric radius,
(3) for the same N_p, the error e between the computed solution and the analytical one increases with the solid volume fraction ϕ, which implies that a much higher resolution is required for dense particulate systems, e.g. a packed bed, than for dilute ones.

The second test case is similar except that the layout of spheres is random. This problem has been studied in Van der Hoef et al. (2005) and Hill et al. (2001a) with a LBM in viscous regime ($\mathcal{R}e < 0.2$). Our simulations are performed for $(\mathcal{R}e, N_p, \Delta t) = (0.01, 16, 0.01)$. For each ϕ we generate five random layouts of particles and the mean velocity V is then averaged over these five configurations. The resulting flow field is illustrated in Fig. 4(a) for $\phi = 0.524$. As for a structured array of spheres, we compute the mean drag coefficient on each sphere K and compare our values with the predictions in Van der Hoef et al. (2005) and Hill et al. (2001a). The agreement with the LBM predictions is very good, as shown in Fig. 4(b), and our computed solution converges linearly with N_p, i.e. as $O(N_p^{-1})$ (not presented here for the sake of conciseness). The same ϕ dependence is observed in the convergence plots: dense systems requires a finer mesh than dilute ones for the same accuracy.

Our third and last test case is the flow through a semi-infinite structured array of spheres at $(\mathcal{R}e, \phi) = (18, \pi/6)$. The objective is to evidence that PeliGRIFF not only supplies accurate solutions in a Stokes flow but also in finite $\mathcal{R}e$ ones, i.e., regimes in which inertia is non-negligible. This test case is well documented in Kanarska et al.

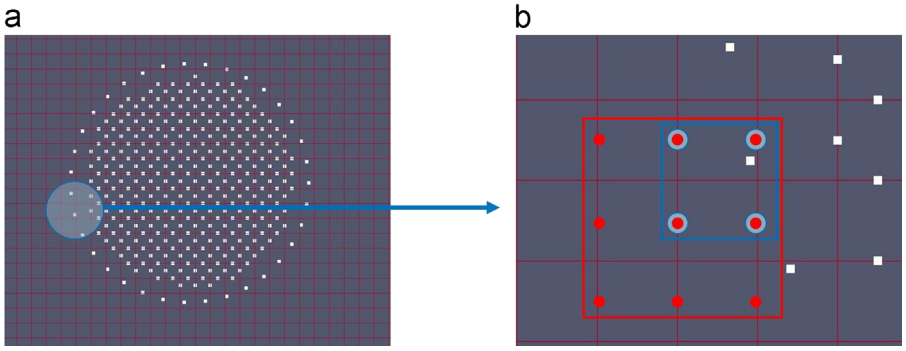

Fig. 2. DLM/FD points on the staggered grid for a 2D circular cylinder: (a) the set of interior and boundary points and (b) in blue the 4-point multi-linear interpolation stencil and in red the 9-point Q2 outwards-oriented quadratic interpolation stencil for the x velocity component. (For interpretation of the references to color in this figure caption, the reader is referred to the web version of this article.)

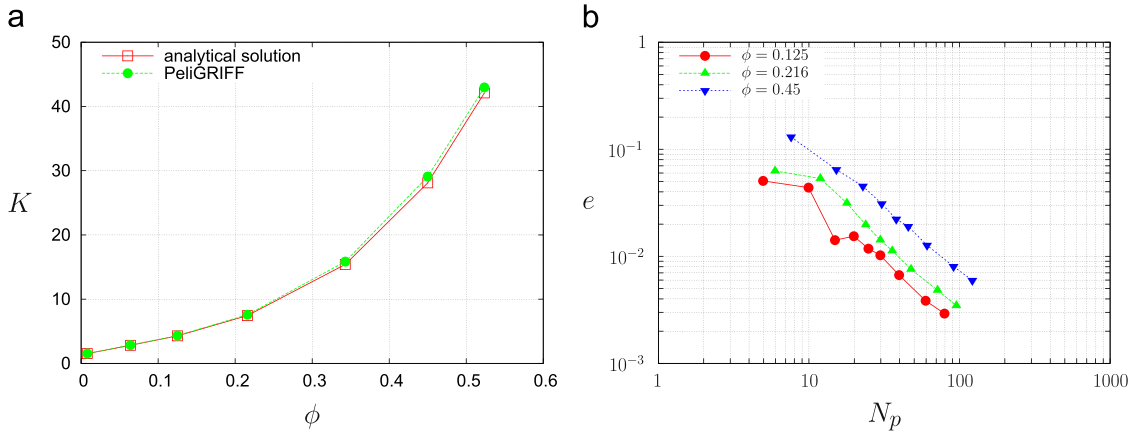

Fig. 3. Comparison of PeliGRIFF results with the analytical solution of Zick and Homsy for the case of the flow through an infinite structured cubic-centered array of spheres at $\mathcal{R}e = 0$: (a) evolution of the drag coefficient K as a function of the solid volume fraction ϕ and (b) convergence of the computed solution as a function of the number of points per particle diameter N_p for increasing solid volume fraction ϕ.

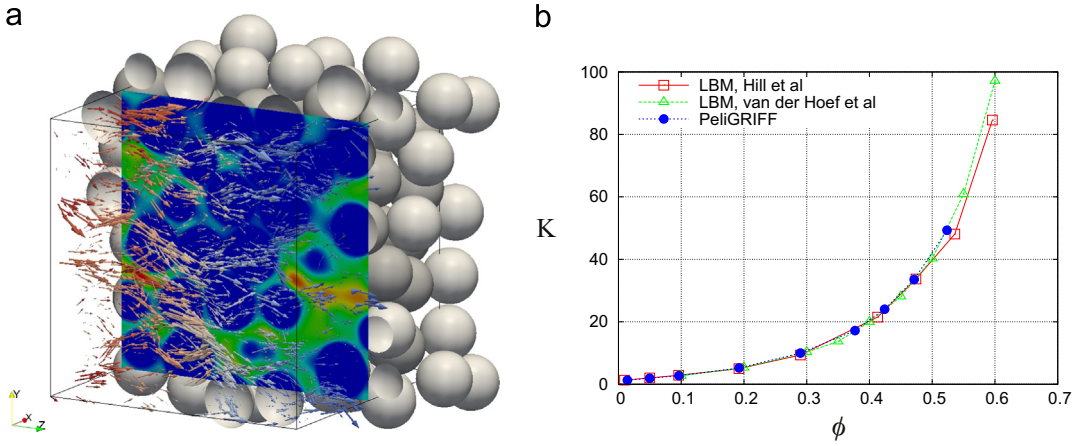

Fig. 4. Stokes flow through a random array of spheres: (a) porous media structure and flow field at $\phi = 0.524$ (front half domain: dimensionless velocity vectors, behind half domain: particles layout, cut plane: contours of dimensionless velocity magnitude, from 0 (blue) to maximum (red)) and (b) mean drag coefficient K on a sphere, comparison with other works of the literature. (For interpretation of the references to color in this figure caption, the reader is referred to the web version of this article.)

(2011), it consists of a structured bed of 12 particles laid out as $3 \times 2 \times 2$ in the (x, y, z) frame. Periodic boundary conditions in the y and z directions model the semi-infinite configuration. The computational domain is bounded by entry and exit zones in the x direction (the direction of the flow). These two zones span one particle diameter d^* such that the total computational domain dimensions are $4d^* \times 2d^* \times 2d^*$. At the inlet boundary, a constant velocity field $(U^*, 0, 0)$ is imposed while classical outflow boundary conditions with a reference constant pressure (set to 0 for convenience purposes) are applied at the exit plane. Different computations with an increasing N_p are performed: 8, 16, 20, 24, 32, 48, 64, 96, 128, 160 (the largest N_p value, i.e. 160, implies a mesh comprising $640 \times 320 \times 320 \simeq 65$ million of cells and ran on 128 cores of a supercomputer). Fig. 5(a) illustrates the flow field in the xz symmetry plane while Fig. 5(b) plots the convergence of the computed solution with mesh refinement. The solution converges as $N_p^{-1.65}$ and the error is less than 4% from $N_p = 32$ (note that the error is computed with the Richardson extrapolation to infinite N_p as the reference solution). The friction coefficient Λ is defined as in Kanarska et al. (2011):

$$\Lambda = \frac{\Delta P^*}{L^*} \frac{(1-\phi)^3 d^{*2}}{\phi^2 \eta^* U^*} \tag{14}$$

Its value computed by PeliGRIFF is $\Lambda = 182$, in line with the numerical prediction of Kanarska et al. (2011) and the assorted correlations considered therein.

3. Results

3.1. Assessment of the accuracy of the computed solution for the case of a random array of cylinders

Prior to examining the flow through a packed bed of cylinders, we first assess the accuracy of the computed solution in such a configuration. Though we thoroughly studied it in the case of spheres, there is no certainty that the rule in terms of number of points per diameter derived for spheres is still valid for cylinders. In fact, cylinders exhibit sharp edges and hence the flow field is tougher to capture in a proper way. For the sake of clarity, let us introduce the height H^* to diameter d^* ratio $a_r = H^*/d^*$ of a cylinder.

Thus, we first consider a small bed made of 20 mono-disperse cylinders with $a_r = 1.875$ (dimensionally $H^* = 3$ mm and $d^* = 1.6$ mm) in a computational domain with the following boundary conditions (see Fig. 6(a)):

- periodic boundary conditions in the transverse (horizontal) directions to the main flow,
- a uniform inlet (upward oriented) velocity at the bottom wall,
- free outflow at the top wall (reference pressure set to 0 and homogeneous Neumann boundary conditions for all velocity components).

The computational domain dimensions are $11.25d^* \times 3.75d^* \times 3.75d^*$ (dimensionally 18 mm × 6 mm × 6 mm) and the bottom

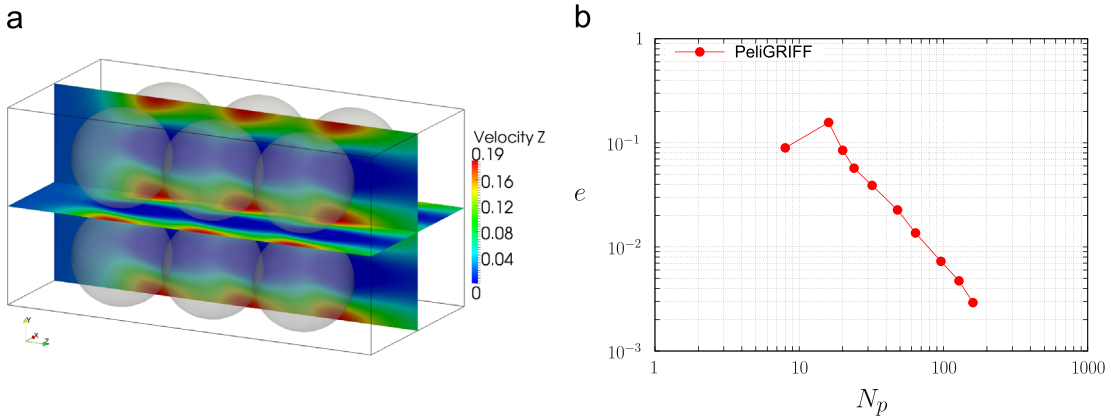

Fig. 5. Flow though a semi-infinite structured array of spheres at $\mathcal{R}e = 18$: (a) flow field (streamwise velocity component, in m/s) and (b) convergence of the computed solution as a function of the number of points per particle diameter N_p.

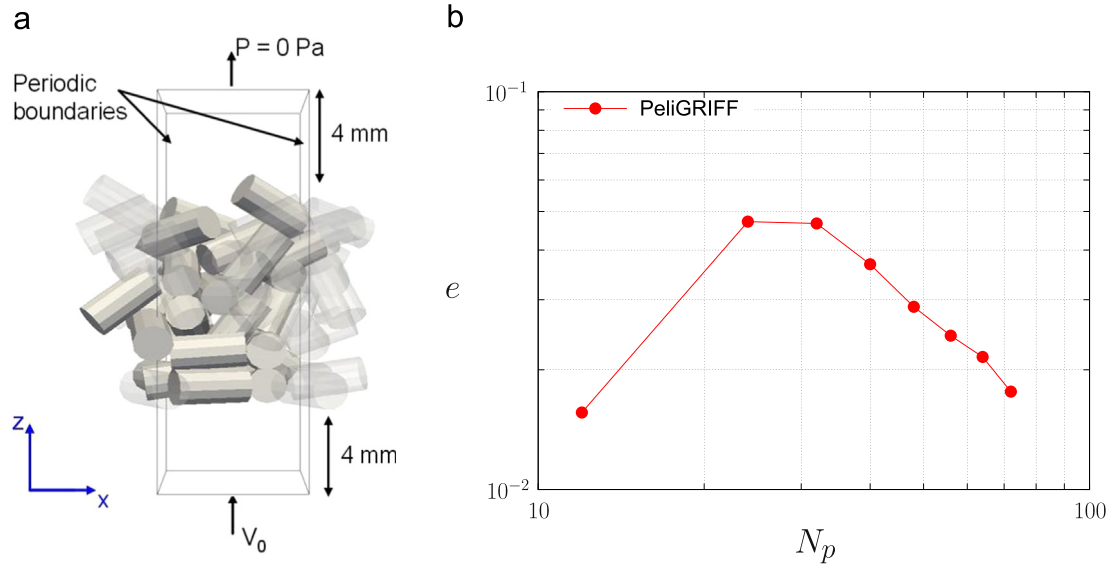

Fig. 6. A small bed of mono-disperse cylinders to assess the accuracy of the computed solution: (a) domain and boundary conditions (note: transparent particles are periodic particles) and, (b) convergence of the computed solution as a function of the number of points per cylinder diameter N_p.

of the packed bed is located at $2.5d^*$ (dimensionally 4 mm) from the inlet bottom wall. The bed of 20 cylinders is the result of a dynamic granular simulation similar to the one employed in Section 3.2. The approximate value of ϕ is 0.6. In all simulations, the particulate Reynolds number $\mathcal{R}e$ is set to 0.43. As for spheres in Section 2.3, different computations with an increasing number of points per cylinder diameter N_p: 24, 32, 40, 48, 56, 64, 72, are performed. The last case $N_p = 72$ corresponds to a computational domain composed of $270 \times 270 \times 810 \simeq 60$ million of cells and run on 128 cores of a supercomputer. Once again, we look at the convergence of the friction coefficent Λ as a function of N_p. Obtained results are plotted in Fig. 6(b) and highlight a convergence in $N_p^{-1.15}$, i.e., slightly better than linear. The convergence rate for cylinders is less than the one for spheres, as expected, since the problem is geometrically stiffer. However, convergence is achieved. Also, Fig. 6(b) reveals that a larger number N_p is required for cylinders than for spheres for an equivalent accuracy. The outcome is clear: not only the solution converges slower for cylinders than spheres but the magnitude of the error is larger for the same N_p. Computing the flow through a packed bed of cylinders requires an approximately 50% finer mesh than for a packed bed of spheres for an equivalent accuracy, which translates into $1.5^3 \simeq 4-$fold more cells, i.e., a 4 folds larger computing cost. From $N_p = 40$, the error is less than 4% and in the following all presented results are obtained with a $N_p = 40$ mesh.

3.2. Effect of size distribution on the pressure drop through a bed of poly-disperse cylinders

Our final goal is to examine the flow through a packed bed of poly-disperse cylinders. The configuration is similar to the one adopted in Section 3.1 but the bed height is larger. In fact, the computational domain height is fixed to 48 mm with entry and exit lengths of 4 mm, thus the bed itself is approximately 40 mm high in all the cases. We consider three classes of cylinders of diameter 1.6 mm and increasing length 2 mm, 3 mm and 4 mm, called L2, L3 and L4 respectively. Two poly-disperse distributions centered on L3 are selected: L234-25/50/25 and L234-40/20/40 that comprise 25% of L2, 50% of L3 and 25% of L4, and 40% of L2, 20% of L3 and 40% of L4, respectively. For comparison purposes, we perform additional simulations in the following configurations:

- mono-disperse beds of cylinders L2, L3 and L4,
- mono-disperse beds of spheres of equivalent diameter to L2, L3 and L4 (equivalent diameter meaning here that spheres have

the same volume as corresponding cylinders), called S2, S3 and S4 respectively,
- poly-disperse beds of spheres S2, S3 and S4 with similar distribution.

For each configuration, we run three simulations with varying microstructure. To do so, the bed of pellets is created by randomly seeding them at the top of the domain and letting them settle under gravity and contact until a motionless packed bed is obtained. These granular dynamics simulations are performed with the soft-sphere DEM code Grains3D (Wachs et al., 2012), which is also employed as the collision algorithm in freely moving particles simulations (Wachs, 2009, 2011). This enables us to calculate a meaningful mean value of the pressure drop (Van der Hoef et al., 2005) as well as to estimate the variability of the flow associated to the local microstructure of the bed of pellets. Grains3D has been validated for cylinders of small a_r in Wachs et al. (2012) and additional comparisons with Leva and Grummer (1947) for similar a_r as here but in a walled domain (tube) instead of a bi-periodic one have shown reasonable agreement (see Dorai et al., 2012b; Dorai, 2014 for more detail about the analysis of the microstructure of packed beds of cylinders).

Fig. 7 illustrates the microstructure of the mono-disperse and poly-disperse beds of cylindrical pellets. In our simulations, the bed height to pellet length ratio varies from 10 to 20. This is rather small and inlet and outlet length effects are non-negligible in the pressure drop calculation. Besides, it is rather hard to determine in a reliable way the actual height of the bed (see the free surface of particles in Fig. 7) and hence the corresponding porosity. Therefore, the method adopted to extract the pressure drop across the bed from our simulation results is the following: we consider a sub-domain in the vertical direction in the core of the bed that corresponds to discarding approximately one pellet length both at the entry and exit of the bed. The local porosity in this sub-domain is numerically computed using the fluid mesh and subdividing cells that are sliced by a pellet boundary into sub-cells. From 4 sub-divisions, we verified on known solutions, e.g., a single cylinder in a box, that this method provides porosity estimates with less than 0.1% error, which is deemed to be very satisfactory.

Further examining the microstructure, we compute the mean orientation of cylinders in the packed beds. Since cylinders have an aspect ratio a_r larger than 1 and are packed by settling under gravity, they have a tendency to align their axis with the xy horizontal plane. Indeed, the average angle θ_{xy} of cylinders' axis with the xy horizontal plane is around $25-30^\circ$ in all the cases investigated here (including mono and poly-disperse beds). For mono-disperse beds, we note that the larger a_r, the lower θ_{xy}, as expected. Since the domain is bi-periodic, the orientation in the xy horizontal plane, measured as the angle between the cylinders' axis projected in the xy horizontal plane and either the x or y direction, is evenly distributed. It is important to emphasize the particular microstructure of our beds since it has an impact on the pressure drop. However, including the effect of the mean orientation of the cylinders is beyond the scope of this paper, as constructing packed beds of cylindrical particles with a controlled microstructure (both porosity and orientation) remains a daunting task.

In all simulations, inlet velocity U^* and fluid viscosity η^* are adjusted such that the corresponding particulate Reynolds number is approximately $\mathcal{R}e \simeq 0.4$. Hence, all simulations are performed in the Stokes (viscous) regime. Using $N_p=40$ leads to a mesh that comprises $150\times150\times1200=27$ million of cells. Jobs are run on 64 cores on a supercomputer. The dimensionless time step is set to 0.005. Simulations are run using a transient algorithm from a quiescent initial state until a steady state is reached. The average computing time is around 3 days.

3.2.1. Ergun's correlation in Stokes regimes for mono-disperse pellets

The most classical and widely employed relation giving the pressure drop over a bed as a function of the inlet velocity U^*, local porosity ϵ, particle diameter d^*, fluid viscosity η^* and density ρ_f^* has been suggested by Ergun (1952) that reads

$$\frac{\Delta P^*}{L^*}=A\frac{\eta^*(1-\epsilon)^2U^*}{d^{*2}\epsilon^3}+B\frac{\rho_f^*(1-\epsilon)U^{*2}}{d^*\epsilon^3} \tag{15}$$

A and B are two constants determined from an experimental data fitting procedure. Ergun suggested 150 and 1.75, respectively for a bed of mono-disperse spheres. In Stokes (viscous) regimes ($Re<1$), the latter term in the right-hand-side of (15), i.e. the inertial contribution, can be dropped. Besides, it is generally admitted (see, e.g., Nemec and Levec, 2005 among many others) that (15) under-predicts the pressure drop in Stokes regimes and

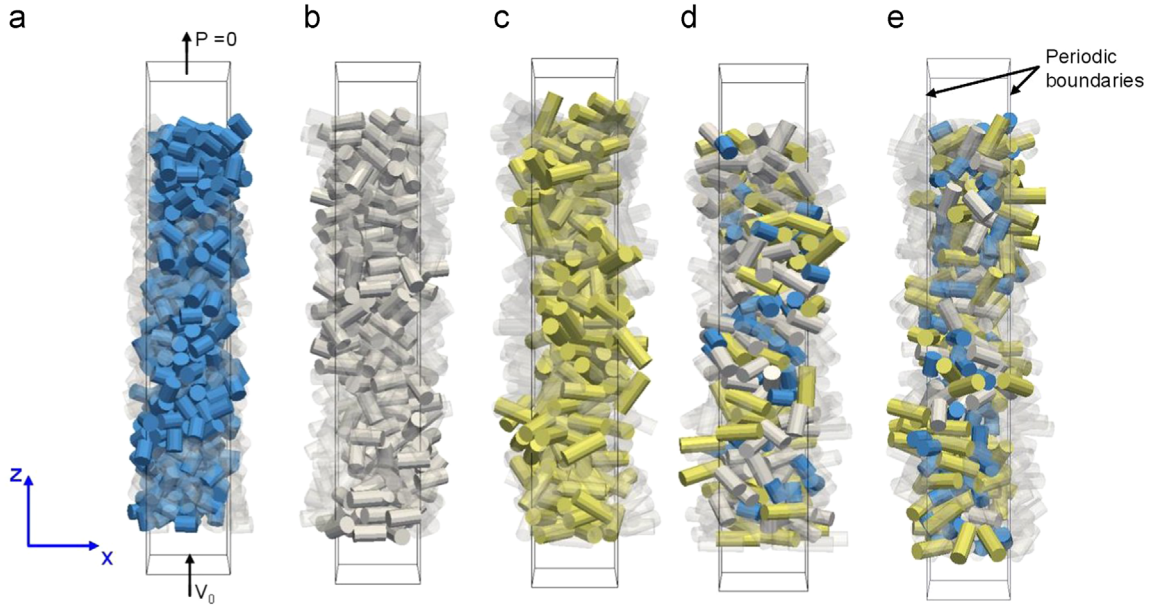

Fig. 7. Packed beds of cylinders: (a) blue particles L2, (b) grey particles L3, (c) yellow particles L4, (d) L234-25/50/25 distribution and (e) L234-40/20/40 distribution (transparent particles=periodic particles). (For interpretation of the references to color in this figure caption, the reader is referred to the web version of this article.)

Carman (1937) suggested $A=180$ as a better match. In the present work, we focus on the viscous regime since $\mathcal{R}e \simeq 0.4$ in our simulations. Computed dimensionless pressure drops Γ defined as $(\Delta P^*/L^*)/(\eta^* U^*/d^{*2})$ are plotted in Fig. 8 as a function of the porosity ϵ for the 9 PeliGRIFF simulations (3 different microstructures for each S_i, $i \in \langle 2,4 \rangle$) together with Ergun's and Carman's correlations. For each spherical particle diameter S_i, both the 3 values related to different microstructure and the mean porosity – mean Γ are shown. Overall, mean values exhibit a much better agreement with Carman's correlation than with Ergun's, as expected in a viscous regime. Interestingly, in the small system we considered (especially in the direction transverse to the flow which spans a few particle diameters only), the variability of the microstructure is rather noticeable and its impact on the pressure drops significantly in relation to the ϵ dependence of Ergun's relation. In other words, small variations of the local porosity of the bed lead to large variations of the pressure drop in a loosely packed bed. Fig. 8 indicates that for the same system, relative variations of ϵ around its mean value up to 1.5% results in almost 10% similar relative variations for the dimensionless pressure drop Γ. This remarkably emphasizes the local microstructure effects in small scale bed of particles, even for spherical and mono-disperse shapes. Based on average values, the fully resolved predictions of PeliGRIFF of the pressure drop through the bed are 3% less than Carman's correlation, which confirms that Carman'scorrelation supplies a reliable and reasonably good estimate of the pressure drop in the viscous regime, while conversely we confirm that Ergun's markedly under-predicts it, as already suggested in the literature (Hill et al., 2001b; Nemec and Levec, 2005). Fitting our results provide $A \simeq 175$.

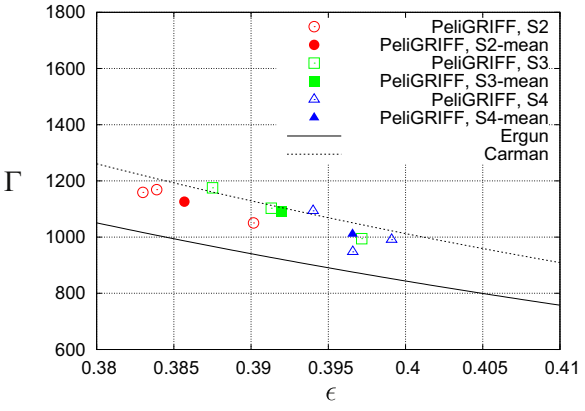

Fig. 8. Comparison of $\Gamma = (\Delta P^*/L^*)/(\eta^* U^* d^{*2})$ obtained by PeliGRIFF for a bed of mono-disperse spheres as a function of the porosity ϵ with Ergun's and Carman's correlations.

We now consider beds of mono-disperse cylinders with constant diameter and 3 different lengths L2, L3 and L4. Previous works in the literature (Niven, 2002; Nemec and Levec, 2005) advocated to modify the classical Ergun's correlation for non-spherical particles by introducing the following additional parameters:

- the particle sphericity φ_p defined as

$$\varphi_p = \frac{A^*_{es}}{A^*_p} = \left(\frac{36\pi V^{*2}_p}{A^{*3}_p}\right)^{1/3} \tag{16}$$

  where A^*_{es}, A^*_p and V^*_p denote the surface area of the equivalent volume sphere, the surface area of the particle and the particle volume, respectively.
- the diameter of the arbitrarily shaped particle d^*_p defined as

$$d^*_p = \frac{6V^*_p}{A^*_p} \tag{17}$$

- the equivalent volume sphere diameter d^*_{es} defined as

$$d^*_{es} = \frac{6V^*_p}{A^*_{es}} = \left(\frac{6V^*_p}{\pi}\right)^{1/3} = \frac{d^*_p}{\varphi_p} \tag{18}$$

- a φ_p-dependent Ergun constant $A(\varphi_p)$

Thus, the modified Ergun's correlation in the viscous regime for non-spherical particles reads (Nemec and Levec, 2005):

$$\frac{\Delta P^*}{L^*} = A(\varphi_p)\frac{\eta^*(1-\epsilon)^2 U^*}{d^{*2}_p \epsilon^3} \tag{19}$$

In Nemec and Levec (2005), the authors suggest the following relation for cylinders:

$$A(\varphi_p) = \frac{150}{\varphi_p^{3/2}} \tag{20}$$

based on a fitting procedure on a rather limited number of experimental data in a laminar-inertial regime $1 < \mathcal{R}e < 1000$. It is also worth observing that though reasonably good, (20) is up to 10% off from the experimental data for certain cylinder aspect ratio (see Nemec and Levec, 2005, Fig. 2(a)). In Fig. 9(a), the dimensionless pressure drop computed by PeliGRIFF for the three classes of cylinders L2, L3 and L4 together with the Ergun's correlation modified for cylinders suggested in Nemec and Levec (2005) is

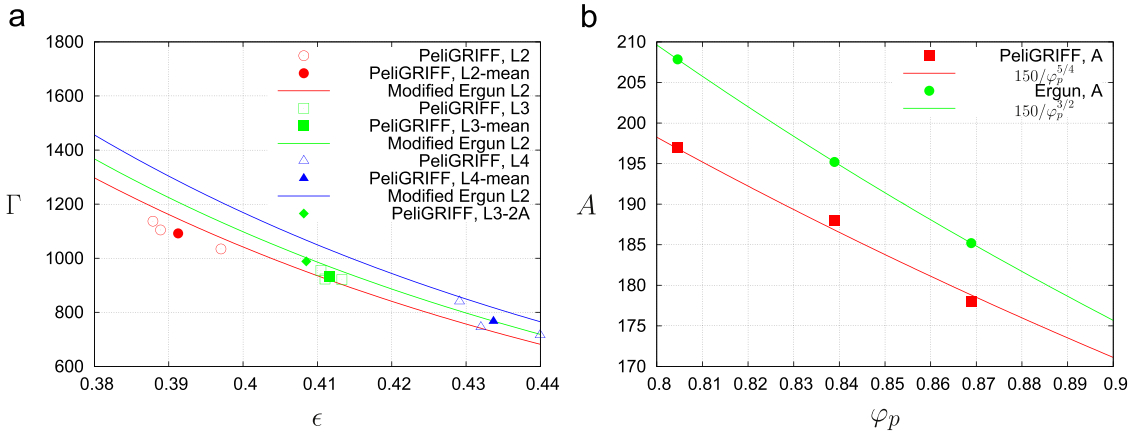

Fig. 9. Pressure drop through a bed of mono-disperse cylinders of varying aspect ratio: (a) $\Gamma = (\Delta P^*/L^*)/(\eta^* U^* d^{*2}_{es})$ as a function of the porosity ϵ, comparison between results computed with PeliGRIFF and the modified Ergun's correlation in the viscous regime and (b) variation of constant A as a function of the sphericity φ_p, correlation fitted using results computed with PeliGRIFF and the one suggested in Nemec and Levec (2005).

plotted. A generally satisfactory agreement is obtained with the maximum difference being of the order of 6% for the highest aspect ratio $a_r=2.5$, as evidenced in Table 1. We also tried to fit our results in terms of variation of the constant A with the sphericity φ_p. In the viscous regime, our results suggest a 5/4 power law variation rather than a 3/2 one, as shown in Fig. 9(b), but this should be considered with care as additional simulations would be suited to confirm this result.

As for spheres, we observe relative deviations around the mean pressure drop value up to 10% due to the different local microstructure resulting from the 3 runs for each class of cylinder. Once again, we confirm that reproducibility of pressure drop estimate (measurement in experiments vs calculation in numerical simulation) is hard to guarantee, or said differently can lead up to 20% ($\pm$10%) change between the lowest and highest values. However, we expected that reproducibility for cylinders would be even worse than for spheres, in relation to their ability to orientate themselves in the bed whereas the isotropy of spheres prevents them from affecting too much the porosity and microstructure of the bed (Nemec and Levec, 2005). We believe that our analysis may be partly biased here by the rather small transverse dimensions of our computational domain (though an additional simulation for a twice larger bi-periodic domain in the L3 case, shown in Fig. 9(a) as a plain green diamond and labelled L3-2A, has yielded a pressure drop within the aforementioned range of scattering). In fact, computed results are markedly more scattered as the ratio between the sphere diameter or cylinder length to the domain transverse length decreases, as evidenced in Fig. 8 for S4 and Fig. 9 (a) for L4 (blue results). Finally, we analyze the impact of the particle shape on the dimensionless pressure drop Γ in Table 2. As expected, the difference between spheres and cylinders increases with the cylinder aspect ratio a_r. From $e_\Gamma(L,S)$, we get the total effect of the particle shape on Γ, as a combination of particles orientation and porosity in the bed. However, it is beneficial to the understanding how the flow through a bed of cylindrical particles differs from the one through a bed of spheres to sort out the effect of porosity from the effect of shape and orientation only, at equivalent porosity. $e_\Gamma(L,S(\overline{\epsilon_L}))$ represents a measure of the effect of particle shape and orientation only, as it compares Γ for each class of cylinders with Γ obtained for a bed of spheres at the same porosity ϵ, extrapolated from the results computed with PeliGRIFF for spheres. Interestingly, for a low aspect ratio $a_r=1.25$, the resulting porosity is the major factor that affects Γ, while from $a_r=1.875$ the effect of shape and orientation of cylinders and the resulting porosity acts in opposite ways and the former partly compensates the latter (+10.7% vs −24.1%). It is likely that for even higher aspect ratio a_r, the effect of particle shape and orientation will prevail, but this should be verified first.

3.2.2. Extension to poly-disperse pellets

We now report on the results computed for beds of poly-disperse particles. In Van der Hoef et al. (2005) and Beetstra et al. (2007), the authors suggest a correction to the average hydrodynamic force exerted by the fluid on a class of spherical particles

Table 1
Dimensionless mean pressure drop across a bed of mono-disperse cylinders for the three classes considered L2, L3, L4 and comparison with the modified Ergun correlation suggested in Nemec and Levec (2005), where $e_\Gamma(Pel,Erg)=100|\overline{\Gamma_{Pel}}-\overline{\Gamma_{Erg}}|/\overline{\Gamma_{Erg}}$.

Type	a_r	φ_p	$\overline{\epsilon}$	$\overline{\Gamma_{Pel}}$	$\overline{\Gamma_{Erg}}$	$e_\Gamma(Pel,Erg)$
L2	1.25	0.8689	0.391	1092	1147	+4.8
L3	1.875	0.8389	0.412	933	969	+3.7
L4	2.5	0.8046	0.434	767	818	+6.2

Table 2
Dimensionless mean pressure drop across a bed of mono-disperse particles: effect of particle shape from spheres to cylinders, where $e_\Theta(i,j)=100(\overline{\Theta_i}-\overline{\Theta_j})/\overline{\Theta_j}$.

Class	$\overline{\epsilon_{S_i}}$	$\overline{\epsilon_L}$	$e_\epsilon(L,S)$	$\overline{\Gamma_{Pel,S}}$	$\overline{\Gamma_{Pel,L}}$	$e_\Gamma(L,S)$	$\Gamma_{Pel,S(\overline{\epsilon_L})}$	$e_\Gamma(L,S(\overline{\epsilon_L}))$
2	0.386	0.391	1.3	1126	1092	−3.0	1085	+0.6
3	0.392	0.412	5.1	1090	933	−14.4	865	+7.3
4	0.397	0.434	9.3	1010	767	−24.1	685	+10.7

of diameter d_i in a bed of poly-disperse spheres. Following Van der Hoef et al. (2005), the relation between the total dimensional $F^*_{f->s}$ and dimensionless F hydrodynamic force exerted by the fluid on a sphere of diameter d reads:

$$F=\frac{(1-\phi)F^*_{f->s}}{3\pi\eta^* d^* U^*} \tag{21}$$

From a simple balance of force in the domain of volume V^* containing N particles: $V^*(\Delta P^*/L^*)=NF^*_{f->s}$, we get the relation between F and $\Delta P^*/L^*$:

$$F=\frac{1-\phi}{\phi}\frac{d^{*2}}{18\eta^* U^*}\frac{\Delta P^*}{L^*} \tag{22}$$

In other words, from (13), F is nothing else than $(1-\phi)K$. For a bed of poly-disperse spheres, Van der Hoef et al. (2005) and Beetstra et al. (2007) suggested the following correlation obtained by fitting a large number of LBM simulations for the dimensionless hydrodynamic force F_i acting on the class of spheres of diameter d_i:

$$F_i(\phi,\mathcal{R}e_i)=((1-\phi)y_i+\phi y_i^2+0.064(1-\phi)y_i^3)F(\phi,\langle\mathcal{R}e\rangle) \tag{23}$$

where $F(\phi,\langle\mathcal{R}e\rangle)$ is the dimensionless hydrodynamic force for a bed of mono-disperse spheres of diameter d_i at the same global volume fraction ϕ and equivalent Reynolds number $\langle\mathcal{R}e\rangle$. Since we are interested in the viscous regime here, we drop the $\mathcal{R}e$ dependence. In (23), $y_i=d_i^*/\langle d^*\rangle$ where $\langle d^*\rangle$ is the Sauter diameter classically defined as

$$\langle d^*\rangle=\frac{\sum_{i=0}^{c}N_i d_i^{*3}}{\sum_{i=0}^{c}N_i d_i^{*2}} \tag{24}$$

where c denotes the number of classes of spheres. (23) can be translated in terms of pressure drop $\Delta P^*/L^*$ once again starting from the balance of force in the domain for a bed of poly-disperse spheres:

$$V^*\frac{\Delta P^*_{poly}}{L^*}=\sum_{i=0}^{c}N_i F^*_{f->s,i}=\sum_{i=0}^{c}N_i\frac{3\pi\eta^* d_i^* U^*}{1-\phi}F_i(\phi) \tag{25}$$

Introducing the volume of sphere of diameter d_i^* as $V^*_{p,i}=\pi d_i^{*3}/6$ and the volume fraction of class i as $\phi_i=N_i V^*_{p,i}/V^*$, we get

$$\frac{\Delta P^*_{poly}}{L^*}=\sum_{i=0}^{c}\frac{18\eta^* U^*\phi}{(1-\phi)d_i^{*2}}\frac{\phi_i}{\phi}F_i(\phi) \tag{26}$$

Using (23) and $x_i=\phi_i/\phi$, we get

$$\frac{\Delta P^*_{poly}}{L^*}=\sum_{i=0}^{c}\frac{18\eta^* U^*\phi}{(1-\phi)d_i^{*2}}x_i((1-\phi)y_i+\phi y_i^2+0.064(1-\phi)y_i^3)F(\phi) \tag{27}$$

Finally, we have

$$\frac{\Delta P^*_{poly}}{L^*}=\sum_{i=0}^{c}x_i((1-\phi)y_i+\phi y_i^2+0.064(1-\phi)y_i^3)\frac{\Delta P^*_i}{L^*}(\phi) \tag{28}$$

$$\frac{\Delta P^*_i}{L^*}(\phi)=\frac{18\eta^* U^*\phi}{(1-\phi)d_i^{*2}}F(\phi) \tag{29}$$

where $\Delta P^*_i/L^*(\phi)$ corresponds to the pressure drop through a bed of mono-disperse spheres of diameter d_i and volume fraction ϕ. We compare in Table 3 the values of $(\Delta P^*_{poly}L^*)/(\eta^* U^*\langle d^*\rangle^2)$ for the

Table 3
Dimensionless mean pressure drop across a bed of poly-disperse spheres for the two poly-disperse beds considered S234-25/50/25 and S234-40/20/40 and comparison with the correlation suggested in Van der Hoef et al. (2005) and Beetstra et al. (2007), where $e_{\Gamma}(Pel, VdH) = 100(\overline{\Gamma_{Pel}} - \overline{\Gamma_{VdH}})/\overline{\Gamma_{VdH}}$.

Type	$\overline{\Gamma_{Pel}}$	$\overline{\phi_{poly}}$	$\langle d \rangle$	$y_{i \in \langle 2:4 \rangle}$	$x_{i \in \langle 2:4 \rangle}$	$\overline{\Gamma_{VdH}}$	$e_{\Gamma}(Pel, VdH)$
S234-25/50/25	1149	0.6139	0.002272	0.868 0.995 1.092	0.167 0.501 0.332	1174	−2.15
S234-40/20/40	1147	0.6127	0.002278	0.865 0.992 1.088	0.267 0.201 0.532	1152	−0.3

Table 4
Dimensionless mean pressure drop across a bed of poly-disperse cylinders for the two poly-disperse beds considered L234-25/50/25 and L234-40/20/40 and comparison with the correlation suggested in Van der Hoef et al. (2005) and Beetstra et al. (2007) for spheres in which $\langle d \rangle$ and the function $(1-\phi)y_i + \phi y_i^2 + 0.064(1-\phi)y_i^3$ is evaluated with equivalent sphere diameters (i.e. with the same weighting as for S234), where $e_{\Gamma}(Pel, VdH) = 100(\overline{\Gamma_{Pel}} - \overline{\Gamma_{VdH}})/\overline{\Gamma_{VdH}}$.

Type	$\overline{\Gamma_{Pel}}$	$\overline{\phi_{poly}}$	$\langle d \rangle$	$y_{i \in \langle 2:4 \rangle}$	$x_{i \in \langle 2:4 \rangle}$	$\overline{\Gamma_{VdH}}$	$e_{\Gamma}(Pel, VdH)$
L234-25/50/25	1199	0.5785	0.002272	0.868 0.995 1.092	0.167 0.501 0.332	1248	+3.9
L234-40/20/40	1371	0.5847	0.002278	0.865 0.992 1.088	0.267 0.201 0.532	1337	−2.5

two different beds S234-25/50/25 and S234-40/20/40 computed by PeliGRIFF to the reconstructed values based on mono-disperse computed ones $(\Delta P_i^* L^*)/(\eta^* U^* \langle d^* \rangle^2)$ extrapolated to $\overline{\phi_{poly}}$ (using (15) with $A=175$ and $B=0$) and (28). Discrepancies amount to -2.1% and -0.3%, respectively, which is deemed to be very satisfactory. In fact, we get a very good agreement with the work of Van der Hoef et al. (2005), Beetstra et al. (2007), Sarkar et al. (2009) and confirm that their correlation is reliable for our 3-disperse bed (in Van der Hoef et al., 2005; Beetstra et al., 2007, the validity of the proposed correlation is verified for bi-disperse systems while in Sarkar et al., 2009 it is shown to be valid even for a log-normal and Gaussian size distribution).

In Table 4, we gather our computed results for poly-disperse cylinders. Similarly to beds of mono-disperse pellets, poly-disperse cylinders exhibit higher pressure drops than their spherical counterparts. To the best of our knowledge, there does not exist in the literature any correlation for the dimensionless hydrodynamic force and equivalently dimensionless pressure drop for a bed of poly-disperse cylinders. This drove us to test the validity of the correlation of Van der Hoef and co-authors when applied to cylinders. To be more specific, we use (28) in which $(\Delta P_i^*/L^*)(\phi)$ is the value of the pressure drop for the class of cylinder L_i obtained by our code extrapolated to $\overline{\phi_{poly}}$ and $\langle d^* \rangle$ (using (15) with $A = 150/\varphi_p^{5/4}$ and $B=0$) and the function $(1-\phi)y_i + \phi y_i^2 + 0.064(1-\phi)y_i^3$ is calculated using the equivalent volume sphere diameter $d_{es,i}^*$ from (18). In other words, the weights of $(\Delta P_i^*/L^*)(\phi)$ for cylinders L2, L3 and L4 are the same as the ones for the corresponding equivalent volume spheres S2, S3 and S4, respectively. Surprisingly, using this rather coarse approximation (since $(1-\phi)y_i + \phi y_i^2 + 0.064(1-\phi)y_i^3$ does not account for any orientation effect or particle sphericity φ_p) yields reasonably good agreement with less than 4% discrepancy in both cases.

Finally, the variability of the dimensionless pressure drop associated to the different microstructures of the bed in the 3 simulations for each poly-disperse beds is of the same order as for mono-disperse beds, i.e. a maximum of $\pm 10\%$ around the mean value. This statement holds both for spheres and cylinders. And once again, we would like to underline that this rather constant variability in our simulations may be partly biased by the small transverse dimensions of our computational domain.

4. Discussion and perspectives

We have performed fully resolved simulations of the flow through a packed bed of mono and poly-disperse pellets in the viscous regime. We considered both spheres and cylinders. The results on beds made of mono- and poly-disperse cylinders are, to the best of our knowledge, new computational results. The set of computed results enabled us to investigate the global effect of the microstructure of the bed on flow kinematics and pressure drop.

From a computational standpoint, fully resolved simulations of this type of system provide insight into the heart of the flow, with detailed information on local velocity, hydrodynamic forces exerted on individual particles, and so on, but are extremely demanding in terms of computing resources. We have highlighted that accurate and reliable solutions can be obtained while a fine enough mesh is used to discretize the particles. For cylinders, we have shown with an adequate mesh convergence analysis that at least 40 points or cells are necessary over the cylinder diameter at a high volume fraction as the one encountered in a loosely packed bed. This leads to meshes generally comprising a few tens of millions of cells, at least. And hence a numerical tool that scales decently on large supercomputers on up to a few hundreds of cores is suitable.

From an industrial standpoint, we confirm that micro reactors (with classical reactor diameter spanning a few pellet diameters only) have a tendency to be subject to high variability in terms of pressure drop, up to $\pm 10\%$ around the mean value. In our simulations, variability did not change much from spheres to cylinders, though it is reported in the literature (see, e.g., Nemec and Levec, 2005) that it should be higher for cylinders in relation to their ability to orientate themselves in the bed. Though this statement is intuitively correct, we did not find any strong evidence supporting it in our computed results. However, we emphasize once again that the limited transverse dimensions of

our system may affect this observation. In general, the microstructure of our beds of cylinders is characterized by a preferred alignment of cylinders with the plane perpendicular to gravity, and hence all our simulations are performed for a realistic (as our packing process is similar to a real filling of a process engineering catalytic reactor) but specific microstructure. Including explicitly the orientation of the cylinders in the pressure drop correlation is a challenge beyond the scope of this work.

We examined the effect of poly-dispersity both for spheres and cylinders. We remind the reader that in the case of cylinders, the poly-dispersity is created with cylinders of constant diameter but variable length, in an attempt to model realistic process engineering catalytic reactors (in which pellets are produced by extrusion and thus have a constant diameter). However, in our poly-disperse systems, the aspect ratio of the different classes of cylinders is also affected. The considered poly-dispersity hence represents a particular case (examining systems of poly-disperse cylinders of constant aspect ratio may have led to slightly different observations). For the same mass of pellets, cylinders lead to lower pressure drop through the bed essentially because the porosity of the bed of cylinders is larger. And this effect increases as the aspect ratio of the cylinder increases. However, at equivalent porosity, cylinders do dissipate more energy, as one would intuitively expect from their non-smooth shape. We verified, in the viscous regime only, that the correlation proposed by Van der Hoef et al. (2005), Beetstra et al. (2007) and Sarkar et al. (2009) is indeed rather reliable on our 3-disperse beds of spheres. We also examined how valid their correlation would be for poly-disperse cylinders and get unexpectedly good agreement. These are preliminary results only as the number of simulations performed is quite limited so far but it provides plausible clues that the functional form of the correlation $(1-\phi)y_i+\phi y_i^2+0.064(1-\phi)y_i^3$ works quite well for other shapes than spheres, at least at high solid volume fraction. This could potentially have important consequences for the design of catalytic fixed bed reactors.

Future work is two-fold. From a physical standpoint, we will perform additional simulations to provide a pressure drop correlation for beds of poly-disperse cylinders inspired by Van der Hoef et al. (2005), Beetstra et al. (2007) and Sarkar et al. (2009), investigate more quantitatively how much the periodic length of the domain affects our results, add the effect of the reactor wall (localized high porosity) in an attempt to model realistic micro-reactors and examine the local effects of the microstructure (cylinder orientation) on velocity distribution and pressure drop. We have recently extended the simulation capabilities of our granular code Grains3D towards non-convex pellet shape using a glued convex approach (this work will soon be published in a separate paper). Once coupled to our fluid solver PeliGRIFF (and this should be rather straightforward as our DLM/FDM is not sensitive to convexity or concavity), being able to deal with non-convex shapes will enable us to look at the flow through a packed bed of multi-lobed extrudates and cylinders with holes, which have been getting rather popular in catalytic processes over the last decade. However, the more complex the shape, the finer the mesh, which puts more pressure on computational efficiency and requires even larger computing resources. From a numerical development of the fluid model standpoint, the next stage is to implement additional advection-diffusion-reaction conservation equations for the chemical species and address the impact of the coupling between hydrodynamics and chemical reactions on the overall conversion efficiency of the micro-reactor.

Acknowledgements

This work was granted access to the HPC resources of CINES under the allocations 2013-c20132b6699 and 2014-c20142b6699 made by GENCI.

References

Atmakidis, T., Kenig, E.Y., 2012. Numerical analysis of mass transfer in packed-bed reactors with irregular particle arrangements. Chem. Eng. Sci. 81, 77–83.
Beetstra, R., Van der Hoef, M.A., Kuipers, J.A.M., 2007. Drag force of intermediate Reynolds number flow past mono-and bidisperse arrays of spheres. AIChE J. 53 (2), 489–501.
Breugem, W.P., 2012. A second-order accurate immersed boundary method for fully resolved simulations of particle-laden flows. J. Comput. Phys. 231 (13), 4469–4498.
Carman, P.C., 1937. Fluid flow through granular beds. Trans.—Inst. Chem. Eng. 15, 150–166.
Climent, E., Maxey, M.R., 2003. Numerical simulations of random suspensions at finite Reynolds numbers. Int. J. Multiph. Flow 29 (4), 579–601.
Combest, D.P., Ramachandran, P.A., Dudukovic, M.P., 2012. Interstitial-scale transport in packed beds. In: International Symposia on Chemical Reaction Engineering.
Cundall, P.A., Strack, O.D.L., 1979. A discrete numerical model for granular assemblies. Geotechnique 29 (1), 47–65.
Dagan, G., 1989. Flow and Transport in Porous Formations. Springer-Verlag, Berlin, Germany.
Deen, N.G., Kriebitzsch, S.H.L., van der Hoef, M.A., Kuipers, J.A.M., 2012. Direct numerical simulation of flow and heat transfer in dense fluid-particle systems. Chem. Eng. Sci. 81, 329–344.
Delgado, J.M.P.Q., 2006. A critical review of dispersion in packed beds. Heat Mass Transf. 42, 279–310.
Dixon, A.G., Taskin, M.E., Nijemeisland, M., Stitt, E.H., 2010. CFD method to couple three-dimensional transport and reaction inside catalyst particles to the fixed bed flow field. Ind. Eng. Chem. Res. 49 (19), 9012–9025.
Dorai, F., 2014. Etude numerique des chargements, de l'hydrodynamique et de la reactivite dans des reacteurs pilotes a lits fixes (Ph.D. thesis). Université de Toulouse.
Dorai, F., Rolland, M., Wachs, A., Marcoux, M., Climent, E., 2012a. Packing fixed bed reactors with cylinders: influence of particle length distribution. Procedia Eng. 42, 1454–1468.
Dorai, F., Rolland, M., Wachs, A., Marcoux, M., Climent, E., 2012b. Packing fixed bed reactors with cylinders: influence of particle length distribution. Procedia Eng. 42, 1335–1345.
Dudukovic, M.P., Larachi, F., Mills, P.L., 2002. Multiphase catalytic reactors: a perspective on current knowledge and future trends. Catal. Rev. 44 (1), 123–246.
Dviugys, A., Peters, B., 2001. An approach to simulate the motion of spherical and non-spherical fuel particles in combustion chambers. Granul. Matter 3 (4), 231–266.
Ergun, S., 1952. Fluid flow through packed columns. Chem. Eng. Prog. 48, 89–94.
Gierman, H., 1988. Design of laboratory hydrotreating reactors. Appl. Catal. 43, 277–286.
Giese, M., Rottschafer, K., Vortmeyer, D., 1998. Measured and modelled superficial flow profiles in packed beds with liquid flow. AIChE J. 44 (2), 484–490.
Gilbert, E.G., Johnson, D.W., Keerthi, S.S., 1988. A fast procedure for computing the distance between complex objects in three-dimensional space. IEEE J. Robot. Autom. 4 (2), 193–203.
Glowinski, R., Pan, T.W., Hesla, T.I., Joseph, D.D., 1999. A distributed Lagrange multiplier/fictitious domain method for particulate flows. Int. J. Multiph. Flow 25 (5), 755–794.
Graf von der Schulenburg, D.A., Johns, M.L., 2011. Catalyst effectiveness factor distributions in isothermal packed bed reactors. Chem. Eng. Sci. 66 (13), 3003–3011.
Hill, R.J., Koch, D.L., Ladd, A.J.C., 2001a. The first effects of fluid inertia on flows in ordered and random arrays of spheres. J. Fluid Mech. 448 (2), 213–241.
Hill, R.J., Koch, D.L., Ladd, A.J.C., 2001b. Moderate-Reynolds-number flows in ordered and random arrays of spheres. J. Fluid Mech. 448 (2), 243–278.
Höfler, K., Schwarzer, S., 2000. Navier–Stokes simulation with constraint forces: finite-difference method for particle-laden flows and complex geometries. Phys. Rev. E 61 (June), 7146–7160.
Kanarska, Y., Lomov, I., Antoun, T., 2011. Mesoscale simulations of particulate flows with parallel distributed Lagrange multiplier technique. Comput. Fluids 48, 16–29.
Knox, John H., Parcher, Jon F., 1969. Effect of column to particle diameter ratio on the dispersion of unsorbed solutes in chromatography. Anal. Chem. 41, 1599–1606.
Kodamn, M., Bharadwaj, R., Curtis, J., Hancock, B., Wassgren, C., 2010. Cylindrical object contact detection for use in discrete element method simulations. Part I. Contact detection algorithms. Chem. Eng. Sci. 65 (22), 5852–5862.
Ladd, A.J.C., Verberg, R., 2001. Lattice-Boltzmann simulations of particle–fluid suspensions. J. Stat. Phys. 104 (5), 1191–1251.
Leva, M., Grummer, M., 1947. Pressure drop through packed tubes. 3. Prediction of voids in packed tubes. Chem. Eng. Prog. 43 (12), 713–718.
Nemec, D., Levec, J., 2005. Flow through packed bed reactors. I. Single-phase flow. Chem. Eng. Sci. 60 (24), 6947–6957.
Niven, R.K., 2002. Physical insight into the Ergun and Wen and Yu equations for fluid flow in packed and fluidised beds. Chem. Eng. Sci. 57 (3), 527–534.
Peskin, C.S., 1977. Numerical analysis of blood flow in the heart. J. Comput. Phys. 25 (3), 220–252.

Rahmani, M., Wachs, A., 2014. Free falling and rising of spherical and angular particles. Phys. Fluids 26, 083301.
Rolland, M., 2013. Significant effect of catalyst position and orientation in fixed-beds reactors. In: 9th World Congress of Chemical Engineering, Seoul, Korea.
Sarkar, S., Van der Hoef, M.A., Kuipers, J.A.M., 2009. Fluid-particle interaction from lattice Boltzmann simulations for flow through polydisperse random arrays of spheres. Chem. Eng. Sci. 64 (11), 2683–2691.
Sie, S.T., 1991. Scale effects in laboratory and pilot plant reactors for trickle-flow processes. Rev. Inst. Français du Pétrole 46, 501–515.
Uhlmann, M., 2005. An immersed boundary method with direct forcing for the simulation of particulate flows. J. Comput. Phys. 209 (2), 448–476.
Van den Bergen, G., 1999. A fast and robust GJK implementation for collision detection of convex objects. J. Graph., Gpu, Game Tools 4, 7–25.
Van der Hoef, M.A., Beetstra, R., Kuipers, J.A.M., 2005. Lattice-Boltzmann simulations of low-Reynolds-number flow past mono- and bidisperse arrays of spheres: results for the permeability and drag force. J. Fluid Mech. 528, 233–254.
Wachs, A., 2009. A DEM-DLM/FD method for direct numerical simulation of particulate flows: sedimentation of polygonal isometric particles in a Newtonian fluid with collisions. Comput. Fluids 38 (8), 1608–1628.
Wachs, A., 2011. Rising of 3D catalyst particles in a natural convection dominated flow by a parallel DNS method. Comput. Chem. Eng. 35 (11), 2169–2185.
Wachs, A., Girolami, L., Vinay, G., Ferrer, G., 2012. Grains3D, a flexible DEM approach for particles of arbitrary convex shape. Part I. Numerical model and validations. Powder Technol. 224, 374–389.
Wachs, A., Hammouti, A., Vinay, G., Rahmani, M., 2015. Accuracy of finite volume/staggered grid distributed lagrange multiplier/fictitious domain simulations of particulate flows. Comput. Fluids, in preparation.
Yu, Z., Shao, X., 2007. A direct-forcing fictitious domain method for particulate flows. J. Comput. Phys. 227 (1), 292–314.
Zick, A.A., Homsy, G.M., 1982. Stokes flow through periodic arrays of spheres. J. Fluid Mech. 115 (1), 13–26.